ENHANCING MARINE PROPULSION EFFICIENCY: DESIGN, SIMULATION, AND TESTING OF A HIGH-EFFICIENCY TOROIDAL PROPELLER FOR SOLAR SPLASH COMPETITION

Claire Grover **Henry Morgan** **Jacob Lewis** **Junyi Lin** **Santino Lupica-Tondo**

ABSTRACT

Toroidal propellers are at the forefront of marine propulsion innovation due to their increased efficiencies over traditional propellers. This project seeks to capture these benefits and apply them to the University of Rochester Solar Splash Team's endurance race. A toroidal shaped propeller was designed to improve the open water efficiency of Solar Splash's current traditional propeller. This would allow the Solar Splash boat to travel a further distance in their endurance race with the same power input. Through testing, simulation, and multiple rounds of optimization, a toroidal propeller was manufactured with a higher open water efficiency as proven through simulation. However, despite the promising simulation results, the propeller did not achieve a higher open water efficiency in testing. This project highlights the challenges of translating simulation results to real-world performance and underscores the importance of rigorous testing in propeller design.

PROBLEM DEFINITION

The current endurance propeller efficiency of the UR solar splash boat is insufficient, and they need a solution for competition on June 4th, 2024. The endurance event is held over a closed course and lasts 2 hours. Open water efficiency is defined in Eq.1 where K_t is the thrust coefficient and K_q is the torque coefficient as defined in the testing section. Creating an endurance propeller with higher efficiency than their current model will increase Solar Splash's chances of success in the endurance event.

$$\eta_o = \frac{K_t}{2\pi K_q} \quad (1)$$

REQUIREMENTS, SPECIFICATIONS, DELIVERABLES

Requirements

- Mounting Compatibility: The propeller must fit and can be securely mounted on Solar Splash's existing motor, withstanding operational torque levels.
- Space Envelope Compliance: The propeller shall fit within the defined space envelope of its mount and the testing rig.
- Efficiency Optimization: The propeller's efficiency will be optimized for the motor's most efficient RPM.
- Efficiency Benchmarking: Propeller efficiency must surpass that of the 1915-00 Torqeedo v8/p380 propeller (Solar Splash Propeller as seen in Fig.10a, Appendix B).
- Safety Compliance: Testing setup will adhere to the Safety Guidelines of Mechanical Engineering Department, as listed in Appendix G.
- Emergency Procedures: Emergency shutdown procedures and safety features must be established.
- Data Acquisition: The software can collect and record data on thrust and RPM during tests.
- RPM Range Optimization: The propeller will be optimized to perform across a range of RPMs.
- Torque Adaptability: It must operate efficiently across various torque levels.
- Calibration: Calibration of all instruments for accurate and reliable data collection.

Specifications

The specifications are listed in Table 7, Appendix A.

Deliverables

1. Operational, Full-Size Propeller Prototype: A fully functional prototype propeller that meets the specified requirements and fits the existing motor on the Solar Splash. A detailed work breakdown structure and critical path method are shown in Fig. 28, Fig. 29, Fig. 30, and Table 13, Appendix I.
2. Technical Report with Test Data: A comprehensive document detailing the design, testing procedures, results, and analysis of the propeller's performance.
3. Theory of Operation Manual: A manual that explains the operating principles, installation guide, and maintenance procedures for the propeller.

CONCEPTS

At the beginning of the semester, the team identified two propeller designs and CFD software to support each design. The project could either focus on creating a traditional propeller design that increases efficiency by variating elements such as number, radius, and pitch of the blades, or a novel toroidal propeller.

OpenProp software was explored to support the design and analysis of a traditional propeller. OpenProp allows the user to change parameters defining the number and shape of traditional blades through a MATLAB GUI and from the design calculates the efficiency of the propeller. However, OpenProp requires an estimated thrust and advancement velocity of the boat to calculate efficiency.

Siemens StarCCM+ CFD software was also considered due to its compatibility with NX Siemens. StarCCM+ allows any geometry to be transferred from NX and then a CFD simulation can be built around it. While an advancement velocity is also needed for StarCCM+, the thrust produced by the propeller is an output rather than an input.

The team chose to move forward with StarCCM+ software because thrust is calculated in the simulation and the compatibility with NX streamlines design and simulation. Due to recent research in toroidal propeller design [1], that found high increases in efficiency, the team also decided to focus design on a toroidal shaped propeller.

TESTING RIG SETUP

A 3D model of the testing rig was created in NX, and Finite Element Analysis (FEA) was conducted with Nastran, as shown in Fig. 1, to ensure its structural integrity and durability. A one pager for this analysis is shown in Fig.1, Appendix B. Once the design was finalized, we physically fabricated the testing rig and acquired a cattle trough to contain the water. The rig consists of the Solar Splash motor and battery configuration intended for competition, a cattle trough filled with water, and a uniaxial slider attached to a digital scale. A picture of the cattle trough, motor, motor mount, and digital scale is found in Fig. 6, Appendix B. A picture of the battery configuration is shown in Fig. 7, Appendix B. The motor is mounted on a top plate attached to the slider, extending over the trough using 80/20 Aluminum Extrusions, positioning the propeller at the trough's center at a depth equivalent to its submergence when installed on the Solar Splash boat. A zoomed in view of the motor mount and uniaxial slider is found in Fig. 5, Appendix B.

As seen in Fig. 6, Appendix B, to measure the thrust produced by a propeller, a rope is looped around the motor and is attached to a digital scale. When the motor is activated and the propeller starts propelling water, the motor moves along the slider in the opposite direction due to the reaction force of the propeller's thrust. The rope limits how far the motor can move on the slider to prevent it from hitting the end of it. As the propeller pushes water with various force magnitude, the tension on the rope increases accordingly. This tension is transmitted to the digital scale, causing it to register a mass in kilograms. The value displayed on the digital scale corresponds directly to the thrust produced by the propeller at that moment.

TESTING

When conducting testing, two different procedures were followed to obtain the final efficiency results. In the first procedure, the Vedder Electronic Speed Controller (VESC) tool was utilized to gather data. VESC is a controller that draws a certain amperage from the batteries to run the electric motor. VESC would then output a corresponding EPRM for each amperage. ERPM is an electrical measurement and therefore it was necessary to convert ERPM to RPM of the motor using Eq. 2. The Solar Splash motor has 14 poles so therefore there are 7 motor pole pairs.

$$\mathrm{RPM}_{\mathrm{motor}} = \frac{\mathrm{ERPM}}{\mathrm{Motor\ Pole\ Pairs}} \tag{2}$$

$$\mathrm{RPM}_{\mathrm{prop}} = 0.58\mathrm{RPM}_{\mathrm{motor}} \tag{3}$$

After finding the RPM of the motor we used the ratio between the number of drive shaft revolutions for one revolution of the propeller to convert to RPM of the propeller. The Solar Splash 2019 Technical Report recorded this ratio as 0.58 [2]. RPM of the prop is calculated using the RPM of the motor and the gear ratio using Eq. 3. This conversion ensured that our RPM readings accurately represented the propeller's rotational speed. By conducting this test, we were able to measure the thrust values generated by the propeller for each RPM. According to the open water efficiency equation in Eq. 1, thrust T is necessary to calculate efficiency. The coefficient of thrust K_T formula is shown in Eq. 4 where D is the diameter of the propeller and n is the RPM of the propeller.

$$K_T = \frac{T}{\rho n^2 D^4} \tag{4}$$

However, with this procedure the torque is not able to be calculated. Therefore, we are only able to identify the optimal amperage level at which the propeller produced maximum thrust. Testing was limited to a sequence of amperage values between 0 and 22.5, which was the maximum amperage VESC was able to draw from the batteries.

The second procedure involved a setup consisting of a power drill and a push-pull scale to measure torque and thrust across various RPMs simultaneously. Pictures of the test being conducted are found in Fig. 8 and Fig. 9, Appendix B. To conduct this test, we attached a power drill to the coupling of the motor. When the trigger of the power drill was pushed, it rotated the propeller. As the propeller rotated, it exerted a force on the water, causing a reaction force that tried to rotate the power drill in the opposite direction. To measure this resistance, which represents the torque generated by the motor, we applied a push-pull scale to the end of the power drill. The push-pull scale registered the amount of force F required to resist the rotational motion of the power drill. Torque (Q) can be found from this force using Eq. 5 where the perpendicular distance d is 0.1651m.

$$Q = Fd \tag{5}$$

Repeating this process for various RPM values allowed us to collect a range of torque measurements. These measurements were necessary to calculate the coefficient of torque K_Q which is needed to calculate open water efficiency in Eq. 1. The coefficient of torque equation is shown in Eq. 6 where density of the water ρ is 998.67 kg/m^3, Q is torque, RPM of the propeller is n, and diameter of the propeller is D.

$$K_Q = \frac{Q}{\rho n^2 D^5} \quad (6)$$

The torque is measured in testing, n is output from VESC and converted using Eq. 2 and Eq. 3, and D is measured from NX.

The first tests were done to ensure accurate results from the testing rig, correlate the CFD simulation results and the testing rig results, and assess the performance of different propeller materials. The team was unable to conduct the method of measuring torque until the optimization phase, so the first testing procedure was used up until the optimization phase.

First, the thrust produced by the real Solar Splash propeller was tested at varying RPMs. Then the test was repeated, and results were compared in Fig. 11, Appendix C to validate the testing rig's accuracy. Following this, the Solar Splash Propeller was 3D scanned and a point cloud was created in NX Siemens. This scanned geometry was 3D printed to make a replica for further testing. The data from testing the actual propeller was then compared to the 3D printed replica to assess the performance of different materials as seen in Fig. 12, Appendix C. This figure shows a decrease in thrust produced between the actual and 3D printed propellers of 61% at 300RPM. There is a large range in RPMs in testing and this thrust decrease is representative of a middle RPM value. The team expects the 3D printed propeller will perform closer to the actual propeller at low RPM values as the pressure on the blades will decrease and deflection will decrease. It will still be lower due to the poorer surface finish on the 3D printed propeller. Accordingly, at higher RPMs, the 3D printed blades will experience higher deformation and lower thrust will be produced compared to a manufactured version. The results from the 3D printed Solar Splash test was then compared to Solar Splash simulation results in Fig. 13, Appendix C as referenced more in the computational fluid dynamics analysis section.

Next, a baseline toroidal propeller was designed, printed, and tested as seen in Fig. 10b, Appendix B using Siemens NX, comparing its actual performance in RPM vs. Thrust to simulation results in Fig. 14, Appendix C. Furthermore, the Solar Splash propeller shown in Fig. 10a, was compared to the baseline toroidal propeller in terms of RPM vs Thrust in Fig. 15, Appendix C.

COMPUTATIONAL FLUID DYNAMICS (CFD) ANALYSIS

The CFD analysis for this project was based on a tutorial provided by Simcenter STAR-CCM+ User Guide [3]. This tutorial simulates a marine propeller in open water. The simulation also calculates the open water efficiency in Eq. 1, which was the parameter chosen to correlate the simulation to testing results. Several changes were made to the tutorial to reflect the needs of this project.

The most important of these changes is the geometry to be loaded into the simulation. As previously described in the testing section of this report, the toroidal propeller design underwent multiple rounds of optimization to improve its open water efficiency. Therefore, the simulation had to be adaptable to each new iteration. To achieve this, an assembly was created in NX consisting of a rotating region and static region. As seen in Fig. 17, Appendix D, the rotating region consists of a cylinder encompassing the blades and hub of the propeller with the bottom face of the hub placed on the circular face of the cylinder. As seen in Fig. 18a, Appendix D, the static region consists of the shaft, a block defining the limits of the simulation, and a cylindrical subtraction where the rotating region will be placed. As seen in Fig. 18b, Appendix D, when the rotating region is placed inside the static region, the base of the hub directly interfaces with the shaft. The face of the block directly across from the front of the propeller is the velocity inlet, the face directly behind the propeller is the pressure outlet, and the remaining faces are labeled the interface and are the boundaries of the simulation.

Each new propeller design can be input into the rotating region without affecting the rest of the set up. The relevant parameters of the propeller can be selected and transferred along with the geometry directly from NX to StarCCM+. Once the geometry is established, the tutorial's preloaded conditions can be matched and then followed. The tutorial walks the user through creating the mesh, setting up boundary conditions, extending the geometry in the upstream and downstream direction, and creating reports for the data. The only change made to this tutorial was creating a denser mesh around the toroidal propeller rotating region to accurately capture the flow conditions. The far field target surface size of each element was reduced from 1600% of the base size to 800%. The size of the mesh in a cylindrical area encompassing the rotating region was decreased from 50% to 40% relative to the base size.

The simulation differs from the testing set up because it includes a flow of water past the propeller as it is rotating – hence the open water efficiency benchmark. Since Solar Splash was unable to provide data on the target speed for the boat during the endurance race, an approximation was taken using Eq. 7, where VA and L are the advancement velocity and waterline length of the hull in feet, respectively.

$$VA = 1.34 * \sqrt{L_{\text{waterline}}} \quad (7)$$

This formula outputs the hull speed as 5.1 kts, which was then converted to 2.66m/s.

To correlate the results of the simulation with those of testing, the laser-scanned Solar Splash propeller was loaded into the simulation and run at the same RPMs that were measured during a testing session on that propeller. The resulting Thrust vs RPM curves from the simulation and testing data are plotted in Fig. 13, Appendix C. Due to the inclusion of advancement velocity in simulation, the simulated thrust is higher than the measured thrust by a factor of 2.54 at 300rpm.

To predict how future toroidal propeller iterations would perform in testing relative to simulation data, a similar process was done on the baseline toroidal model. This model had undergone no optimization and was 3D printed to correlate testing and simulation data. Once again, the first toroidal propeller model was tested at a range of RPMs and the simulation was run at the same RPMs. The simulated thrust for

the toroidal propeller is higher than the measured thrust by a factor of 1.82 at 300rpm. The variation in simulation and testing data for the toroidal propeller is plotted in Fig. 14, Appendix C.

These factors of increase between testing and simulation thrust data differ by approximately 40%. However, an increase in thrust does not map directly to an increase in efficiency. As seen in Eq. 1, torque must also be considered. At this point in the project the team was not able to test torque. So, to proceed with further propeller designs an assumption was made that since both graphs reflected similar trends, an efficiency improvement in simulation would be reflected by a similar efficiency improvement in testing.

The optimization process is detailed in the Design of Experiments section. Due to the large computational requirements of this process, it was necessary to find a more efficient way to solve each simulation case. This was done using the University of Rochester's BlueHive Cluster from the Center for Integrated Research Computing [4]. This research project was awarded a node on the BlueHive Cluster for two months to streamline analysis and was primarily used for optimization. To further streamline the analysis, the different parameter combinations from the Taguchi arrays described in the DOE section were assembled into simulations. These simulations were then submitted in a batch job to the BlueHive node. The results then had to be post processed to determine the thrust output and efficiency of each design.

Once a final toroidal model was chosen, it was necessary to ensure the manufactured aluminum deliverable would be able to withstand the forces produced by running at a variety of RPMs. To do so, a relative total pressure matrix was outputted from the simulation running at 300 RPM and mapped onto the propeller in NX. A further explanation of this process is found in Appendix G. We expected each blade to perform similarly to a cantilever beam where the greatest deformation is at the end of the blade, because it was fixed at one end, and there was a distributed load acting across from it. An FEA was run using this pressure matrix in Fig. 26, Appendix G to analyze the structural integrity of the propeller. The one pager in Fig. 27, Appendix G indicates that the maximum deflection of the aluminum model was 0.00632 in while the maximum deflection of the plastic model was 0.241 in. The aluminum model deflection is 97% lower than that of the plastic 3D printed model. This, along with the data in Fig. 12, Appendix C as described in the testing section, suggests that the final manufactured model is expected to perform at a higher efficiency than the tests, demonstrating the effectiveness of the design and material choice in withstanding the operational forces.

DESIGN AND OPTIMIZATION

The CAD model for the toroidal propeller was developed in Siemens NX with geometry derived from a 3D scan of the Solar Splash propeller. Initially, the scanned hub of the propeller was kept constant while the toroidal blade design was created by sweeping a body along a guide curve through 3 primary cross sections located at the lead, tip, and tail. The locations, angles, cross-sections shape, and guide curvature at each of these three points were defined by adjustable NX expressions. The independence, range, and number of these parameters continued to develop throughout the project. NACA airfoil curves in the blade cross sections were a major development during the project along with the addition of camber lines to the definitions of the airfoils, shown in Fig. 24, Appendix F.

To analyze the effects of variation among the parameters, designs of experiments were created using Taguchi methods and orthogonal arrays. These experiments minimized the number of simulations runs required to map trends within the parameters. The first experiment utilized a 3rd-order, 4-parameter array where 4 design parameters were tested at 3 values each. This required 9 simulations, producing the results shown in Fig. 19, Appendix E. From there, another equal-size experiment was run in which the lead and tail angles of attack varied less, with the intention of locating the peaks of their response curves. These results are shown in Fig. 20, Appendix E. The third Taguchi experiment was a 3rd-order, 11 parameter experiment focusing on axial angles, blade positions on the hub, and the airfoil characteristics. The resulting efficiency curves for each parameter are shown in Fig. 21, Appendix E. The simulations defined the rotational speed of the rotating region as 5.5 rev/s for all the optimizations. The explanation of this is given in Appendix A.

However, when a simulation was run combining these parameters, the simulated efficiency was significantly lower than other combinations in the orthogonal array. Therefore, the team chose a combination of parameters from the previously created orthogonal arrays that had the highest efficiency to date. These parameters are shown in Table 1. The toroidal propeller with these parameters applied is shown in Fig. 10c, Appendix B. Since only 11 parameters in the model have been optimized, it is likely the model was at a local maximum rather than a global maximum.

TABLE 1
OPTIMUM PARAMETERS FROM TAGUCHI METHOD

Parameter	**Value**
A_AxialAngle_Lead	-10
A_AxialAngle_Tail	0
A_Lead_U	0.75
A_Tail_V	0.2
A_Tangent_Center	6
B_Foil_Thickness_Center	0.2
B_Foil_Thickness_Lead	0.25
B_Foil_Thickness_Tail	0.2
B_Foil_Length_Center	2
B_Foil_Length_Lead	2
B_Foil_Length_Tail	1.375
A_Lead_V	0.6
Efficiency	50.2

To progress in the project, no further optimization of the model was pursued once a local maximum had been identified. The robustness and stability of the local maximum was then examined to ensure the manufactured propeller would perform at a similar efficiency level even with slight variabilities in manufacturing and different operating conditions. Each parameter in Table 1 defining the local maximum was slightly increased and decreased to create two different cases on either side of the maximum. This would indicate what direction the local maximum was more stable in. The two cases and resulting efficiencies are found in Table 2 and Table 3.

TABLE 2
DECREASED OPTIMIZATED PARAMETERS

Parameter	**Value**
A_AxialAngle_Lead	-9
A_AxialAngle_Tail	0
A_Lead_U	0.73
A_Tail_V	0.18
A_Tangent_Center	5.8
B_Foil_Thickness_Center	0.18
B_Foil_Thickness_Lead	0.23
B_Foil_Thickness_Tail	0.18
B_Foil_Length_Center	1.8
B_Foil_Length_Lead	1.8
B_Foil_Length_Tail	1.3
A_Lead_V	0.6
Efficiency	4.76

TABLE 3
INCREASED OPTIMIZED PARAMETERS

Parameter	**Value**
A_AxialAngle_Lead	-11
A_AxialAngle_Tail	1
A_Lead_U	0.77
A_Tail_V	0.22
A_Tangent_Center	6.2
B_Foil_Thickness_Center	0.22
B_Foil_Thickness_Lead	0.27
B_Foil_Thickness_Tail	0.22
B_Foil_Length_Center	2
B_Foil_Length_Lead	2
B_Foil_Length_Tail	1.5
A_Lead_V	0.6
Efficiency	24.5

As seen in the B_Foil_Length_Center and B_Foil_Length_Lead values between Table 1 and Table 3, it was impossible to increase these values without the blades detaching from the hub in the NX model of the propeller. Only the values that were able to be changed in the NX model were altered. Based on the efficiency results from these cases, there is more stability as the parameter values are increased because the efficiency does not drop as much.

To further explore the model's response to points in between the local maximum and the case in Table 3, nine models were created. In each model a parameter was increased to its value in Table 3 while the remaining parameters remained at the Table 1 value. This would indicate which parameters were the greatest drivers of efficiency. The effect each parameter has on efficiency is shown in Fig. 22, Appendix D. The highlighted red line is the baseline efficiency from the local maximum combination to indicate whether than parameter increased or decreased efficiency relative to that run.

While the surface around the local maximum was being mapped, the parameters from Table 1 were added to the NX model and the toroidal propeller was 3D printed to conduct testing simultaneously. While this combination of parameters was the most efficient in simulation, this result was not reflected in testing. The efficiency testing results from this model are shown in Fig. 11 on the top graph. This figure indicates that the toroidal propeller exhibits much lower efficiency over the range of RPMs than the Solar Splash propeller. The team determined this decrease in efficiency was due to the low amount of thrust the toroidal propeller produced, as shown in the bottom graph of Fig. 16, Appendix 16. To account for the fact that efficiency increases in simulation were not being reflected in testing, a constrained optimization based on thrust output was conducted.

Every simulated toroidal model to date was ranked by efficiency and then models that hit the chosen thrust threshold of 170N were pulled. Based on the parameter combinations that created higher thrust values in simulation, a final toroidal model was designed. The final NX CAD model is shown in Fig. 23, Appendix F, and toroidal 3D printed model is shown in Fig. 10d, Appendix B. All defined parameters in this model are shown in Table 4.

TABLE 4
FINAL TOROIDAL PROPELLER PARAMETERS

Parameter	**Values**
A_AOA_Center	15
A_AOA_Lead	45
A_AOA_Tail	200
A_AxialAngle_Lead	-40
A_AxialAngle_Tail	0
A_Blade_Radius	4.4
A_Lead_U	0.85
A_Lead_V	0.65
A_tail_U	0.35
A_Tail_V	0.2
A_Tangent_Center	6
A_Tangent_Lead	15
A_Tangent_Tail	12
B_Foil_Length_Center	2.25
B_Foil_Length_Lead	2.5
B_Foil_Length_Tail	2
B_Foil_Max_Camber_Lead	0.05
B_Foil_Max_Camber_Tail	0.05

B_Foil_Max_Camber_Tip	0
B_Foil_MCamber_Location	0.4
B_Foil_Thickness_Center	0.12
B_Foil_Thickness_Lead	0.12
B_Foil_Thickness_Tail	0.12
C_Airfoil_tail_round	0.02
C_Fillet_radius	0.175

This final model had a much lower simulated efficiency of 1.23, a significant decrease of the 50.1 efficiency shown in the local maximum model. However, the thrust rose to ~268N which increased from the local maximum thrust of ~180N and from the SS propeller thrust of ~200N.

In testing, the final model exhibited higher efficiency and thrust values than the previous toroidal iterations. While it never produced as much thrust as the SS propeller, it was more efficient at lower RPMs.

The Aluminum propeller's thrust and efficiency are expected to be improvements on those of the final 3D printed prototype. The reason for this is an increased stiffness in the aluminum that leads to decreased displacement of the blades, along with the capacity for a smoother surface finish than the 3D print.

MANUFACTURING

In this project, we leveraged CNC manufacturing methods, 3D printing, and basic mechanical fabrication as means of production and testing. 3D printing was particularly suitable for creating complex geometries that would be too intricate or would result in excessive waste if machined. In contrast, CNC machining was employed to produce more durable models that exhibited less deformation during operation.

When it comes to 3D printing, utilizing Polylactic Acid (PLA) offers a more time-efficient and less wasteful approach for developing functional prototypes, especially when compared to CNC machining, which remains ideal for preliminary testing. The printing process for each component required approximately 15 hours, without human intervention during the process. In total, we produced six 3D models for preliminary tests, utilizing the 3D printer at the Rettner Machine Shop at the University of Rochester.

The fabrication process also involves testing rig manufacturing. With the model designed in NX Siemens, engineering drawings of parts are created as seen in Fig. 2, Fig. 3, and Fig. 4, Appendix B and parts were produced with the help of Bill Mildenberger, Taylor Hall Head Machinist. The producing process involved steel processing, measuring, and drilling, which are basic mechanical fabrication processes. Steel was used for its strength. In order to support 50lbs boat outboard during the test and avoid excessive vibration, steel is an optimal choice.

For the final propeller model, Aluminum is the optimal material that we choose due to its ease of manufacturing and better resistance to corrosion, especially in the humid environment compared to steel. We utilized Haas 4-axis CNC machine to manufacture one blade of the toroidal propeller. This involves assistance from Taylor shop manager Bill Mildenberger and Professor Muir to manufacture it. For the full process of development and manufacturing, the cost estimation is produced in Table 5 and Table 6 below:

TABLE 5
COST ESTIMATE TABLE

Item	**Quantity**	**Total Cost**
Aluminum	D 3.5” * 4’	$225
Shop Time	10 hrs	$1000
Team Member Time	10 hrs	$1000
Total Manufacturing Cost		$2225

TABLE 6
DEVELOPMENT TIME ESTIMATE TABLE

Member	**Role**	**Hours**	**Cost**
Claire Grover	Analysis	152.5	$15,250
Henry Morgan	Designing	133.5	$13,350
Jacob Lewis	Testing	89.5	$8,950
Junyi Lin	Manufacturing	102.5	$10,250
Santino Lupica-Tondo	Testing	90	$9,000
Total Development Cost		568	$56,800

For consideration of scaled production, the primary manufacturing method should be changed from CNC to casting to decrease working hours. This change would significantly reduce the unit cost.

RESULTS

Throughout our project, we adapted the initial specifications and requirements in response to practical constraints and data acquisition challenges. These adaptations were critical to maintaining the viability and reliability of our results, given the resources and data available. Table 1, Appendix A clearly reflects whether our system met the established criteria. The obstacles we encountered, including a lack of crucial input from the Solar Splash team, affected our findings and limited our ability to meet the requirements of the project.

Our simulations yielded the Local Maximum Propeller as seen in Fig 10c, Appendix B with nearly the same thrust as the Solar Splash propeller but with significantly greater efficiency. The efficiencies of the Solar Splash and our toroidal propeller were 1.3 and 50.1, respectively, as detailed in Table 1. However, as shown in Table 12, Appendix C, real-world testing did not replicate these figures due to the variance between simulation and actual test conditions.

To mitigate these differences, we applied a constrained optimization approach, ranking the simulated models by efficiency and introducing a thrust baseline of 170N, as specified in our experimental design. Our final model demonstrated a slight reduction in simulated efficiency at 1.23 but generated more simulated thrust than the Solar Splash propeller (approximately 260N versus 200N). This model surpassed prior toroidal designs in actual tests and, although it did not match the Solar Splash propeller’s thrust, it performed with superior power-draw efficiency at reduced RPMs. Table 9, Appendix C shows the efficiency values for the final toroidal model at each amperage while Table 11, Appendix C shows the efficiency

values at each RPM. This data is compared to the efficiency of the Solar Splash propeller at a range of amperages and RPMs in Table 8 and Table 10, Appendix C, respectively.

Our tests indicated that the toroidal propeller as seen in Fig 10d, Appendix B was more efficient at speeds below 250 RPM as shown in the top plot of Fig. 16, Appendix C. The bottom plot of Fig. 16, Appendix C shows that the Solar Splash Propeller and the Toroidal Propeller produced similar thrust.

INTELLECTUAL PROPERTY

Patentability of the Toroidal Propeller Design

The toroidal propeller design developed for the University of Rochester Solar Splash Team's boat presents an approach to enhancing marine propulsion efficiency. This design is characterized by its unique toroidal shape, which significantly improves open water efficiency by optimizing thrust production and reducing the formation of tip vortices, a common issue in traditional propellers.

Relevance to Existing Patents

To determine the patentability of the toroidal propeller design, a comprehensive review of existing patents was conducted. Notable patents in the field of toroidal propeller designs include:

- U.S. Patent US20190135410A1 – Focused on an innovative fluid propulsion system that incorporates a non-traditional blade configuration to enhance hydrodynamic performance and reduce noise. [5]
- U.S. Patent US20140161622A1 – Focused on toroidal propeller's blade design. [6]

Compared to the relevance of existing patents, our design does not have noticeable factors that can be patented. The space has been well patented out.

Companies and Individuals in the Field

Several leading companies and researchers in marine propulsion technology were identified:

- Sharrow Marine: Specializes in high-efficiency marine propellers and has recently explored unconventional shapes to reduce environmental impact.
- Researcher at Massachusetts Institute of Technology: Known for their groundbreaking work in fluid dynamics and propeller design, which includes the development of toroidal-shaped propellers.

Analysis Based on Project IP Assignment

According to the guidelines provided in the project's IP assignment, the design should not only be novel but also non-obvious and capable of industrial application. Our toroidal propeller does not meet these criteria due to its design approach and similarity to existing solutions.

Conclusion and Recommendations

Given the current state of patent saturation in propeller technologies as exemplified by US20190135410A1, it is advisable to focus on developmental improvements and potential licensing strategies instead of pursuing a patent. Collaborating with entities actively researching in this field could provide alternative avenues to leverage the toroidal propeller design commercially or academically.

SOCIETY AND ENVIRONMENTAL IMPLICATIONS

Manufacturing a toroidal propeller for the UR Solar Splash boat can have significant impacts on public health, safety, and welfare, as well as environmental considerations. The toroidal propeller design is particularly beneficial due to its ability to mitigate the formation of tip vortices, which accounts for a sizable portion of the underwater noise pollution generated by typical propellers. By minimizing cavitation and the associated acoustic disturbances, the toroidal propeller creates a quieter underwater environment. This reduction in noise pollution not only enhances the onboard experience for passengers but also mitigates potential noise-induced hearing damage and stress responses in marine life.

The toroidal propeller also exhibits superior hydrodynamic efficiency compared to traditional designs. The diminished tip vortex formation enables the propeller to convert more input energy into thrust, thus requiring less fuel consumption to achieve equivalent propulsion. Lowering fuel consumption subsequently reduces emissions of CO_2, diesel fumes, heavy metals, and other pollutants, positively impacting air quality and public health. However, the manufacturing process for toroidal propellers can be more complex and expensive compared to traditional propellers, posing challenges in scalability and affordability. Ensuring responsible material sourcing and production methods are important to mitigate environmental impacts associated with manufacturing, particularly in terms of energy consumption and waste generation. Ultimately, the integration of toroidal propeller technology into UR Solar Splash represents a step towards cleaner and quieter marine transportation, with associated benefits in terms of health, safety, and environmental sustainability.

RECOMMENDATIONS FOR FUTURE WORK

Testing Limitations

To facilitate the use of Eq. 1 for Open Water Efficiency, our original intention was to utilize the university's water tank, which offers precise speed control. However, the large diameter of the Solar Splash propeller presented a challenge, as it exceeded the tank's capacity. Consequently, we designed and built a custom testing rig using a cattle trough. While this adaptation allowed us to conduct tests, it is important to note that the use of a cattle trough as the tub for testing does not perfectly replicate open water conditions. The water in the trough recirculates, leading to differences in flow patterns compared to open water. Despite this limitation, we were able to gather valuable data on the propeller's performance. However, we were unable to directly measure the advancement coefficient required for Eq.1in this setup. Resolving this limitation should be a priority for future testing efforts to ensure a more accurate assessment of efficiency.

Timeline and Resources

Due to limited timeline and access to Blue Hive, our team was only able to run optimizations on 15 parameters of the roughly 24 defining dimensions. Given more time with Blue Hive, optimization efforts could have been expanded. A more comprehensive approach could have enabled the exploration of a wider range of design possibilities and potentially identify additional local maxima and performance improvements.

Lack of Preliminary Specifications

An additional limitation in this project that leaves room for development was a lack of initial information. Because UR Solar Splash has not competed in several years and the boat was still in early stages of development, critical data was unknown that would have significantly altered the design approach at the onset. In the design of commercial boat propellers, the ideal hull speed and motor performance curves are known. From these, a propeller can be designed that provides the required thrust to maintain desired hull speed and runs at the ideal motor rpm. This propeller is designed with intent to minimize power draw while maintaining these constraints. In this case, ideal hull speed and motor performance curves were unavailable, making the optimization unconstrained, which significantly limits the potential for design improvements. For future work, having this information would support developments beyond what was accomplished here.

Budget

With a larger budget, we would have had the opportunity to 3D print our toroidal propeller using metal, eliminating the need for separate pieces, and creating a more streamlined, single-piece product. This approach would have allowed for greater precision and durability compared to traditional manufacturing methods. Additionally, a fully 3D printed metal propeller would have reduced the risk of assembly errors and potential weak points, resulting in a more robust and efficient final product. The ability to create the propeller as a single, integrated component would have also simplified the manufacturing process, reducing lead times and costs associated with assembly and finishing.

Modeling

The propeller CAD model, while effective, has room for improvement in terms of parameter independence. Complications in geometry and dimensioning in 3D make it challenging to maintain independence between parameters. An example of this is the effect of variation in axial angles on angles of attack. The coordinate system the attack angle rotates from is also defined by axial angle. In practice, this means a change in axial angle causes a slight difference in effective angle of attack. The number of parameters was also kept small to limit the demands placed on optimization. This limited the potential for variation within the model. An example of this is the 3 blade cross-sections. Only defining the cross section at these three points leaves much of the body defined by the software's interpolating method. The blade cross section cannot be made to bulge or shrink in between these defining points.

ACKNOWLEDGMENTS

We would like to extend our sincerest gratitude to several individuals whose contributions have been instrumental in the success of our project. Firstly, a big thank you to Chris Pratt for her exceptional efficiency in ordering and promptly picking up the testing rig tank and aluminum rod. We were amazed by Chris Pratt's quick action; after we asked her to order the materials, she had them to us by the next day.

We are also immensely grateful to Bill Mildenberger for generously allowing us to utilize his space and tools in Taylor to conduct our experiment. Additionally, we thank Bill for his expertise in assembling the aluminum toroidal propeller from the individual pieces we provided. His assistance has been invaluable.

A huge special thanks are due to Jim Alkins for his efforts in 3D printing our propeller models in Rettner. Jim's expertise and dedication have been crucial in bringing our designs to actual models.

We are immensely grateful to Professor Mohammad for his invaluable contributions to our project. His expertise and assistance were instrumental in setting up our simulations and accessing Blue Hive resources. Moreover, his efforts in securing a one-month extension allowed us to refine our designs and conduct thorough testing. Professor Mohammad's guidance during the testing phase was particularly insightful, and his overall advisory role greatly contributed to the success of our project. We truly appreciate his dedication and support throughout this endeavor.

We express our deepest appreciation to Professor Muir for his unwavering support and guidance throughout this project. Professor Muir's dedication, wisdom, and countless hours of assistance have been instrumental in our project. From his help in 3D modeling to his guidance in experimentation, we are grateful for his mentorship and commitment to our success.

REFERENCES

[1] S. Nasiri, S. Peyghami, M. Parniani and F. Blaabjerg, 2021, "An Open-Water Efficiency Based Speed Change Strategy With Propeller Lifespan Enhancement in All-Electric Ships," IEEE, vol. 9, pp. 22595-22604.

[2] "Technical reports," Solar Splash, https://sa.rochester.edu/solarsplash/technical-reports/ (accessed Apr. 28, 2024).

[3] "Simcenter STAR-CCM+ - User Guide (Html)" [Online]. Available: https://docs.sw.siemens.com/en-US/doc/226870983/PL20230724207774020.starccmp_userguide_html?audience=external. [Accessed: 24-Apr-2024].

[4] Computing (CIRC), C. for I. R., "Resources," Center for Integrated Research Computing (CIRC).

[5] T. Sebastian and C. Strem, "Toroidal Propeller," May. 9, 2019

[6] G. C. Sharrow, “Propeller,” Jun. 12, 2014
[7] Earnest Machine Products, 2023, "High-Strength Steel Nylon-Insert Locknut Specification Sheet," [Online]. Available: https://platform.earnestmachine.com/legacy/item-spec-sheets/361006.pdf. [Accessed: 28- Apr- 2024]

APPENDIX A-SPECIFICATIONS

TABLE 7
SPECIFICATIONS OF THE PROJECT, AND IF SYSTEM PASSED SPECIFICATIONS

No.	Value	Units	Description	Method of Evaluation	If System Passed Specification
1	14	in	Maximum diameter of the propeller when mounted on the engine.	Measure the propeller's diameter.	Yes
2	1/2	in	Match the Bore Diameter of propeller mount and locking feature.	Measure the bore diameter of the connection.	Yes
3	N/A	lbf*ft	Must transmit equivalent torque; connection resilience.	Measure torque transmitted through the motor and propeller connection.	Yes
4	10	%	Efficiency improvement over the current propeller.	Calculate the Thrust(lbf)/Mechanical Power(hp) ratio at the most efficient RPM.	No
5	10	%	Operation within the most efficient RPM range of the motor.	Refer to the brushless motor's torque-speed curves.	No
6	10	%	Water tank testing simulates hull speed ranges.	Hull speed calculated by $1.2 \cdot \sqrt{waterline}$.	No

Defining Rotational Speed of the Propeller in Simulations

When deciding on a rotational speed to compare the results between the traditional Solar Splash propeller and each toroidal iteration, it was determined that 300rpm would be sufficient. This speed was chosen because when the first torque measurements were being taken as described in the second testing procedure in the testing section, 300rpm was the only speed that was shared across the Solar Splash and toroidal propeller. It was decided to run all subsequent simulations at this speed so efficiency between both propellers and across testing and simulation could be related.

APPENDIX B-TESTING RIG DRAWING AND ANALYSIS

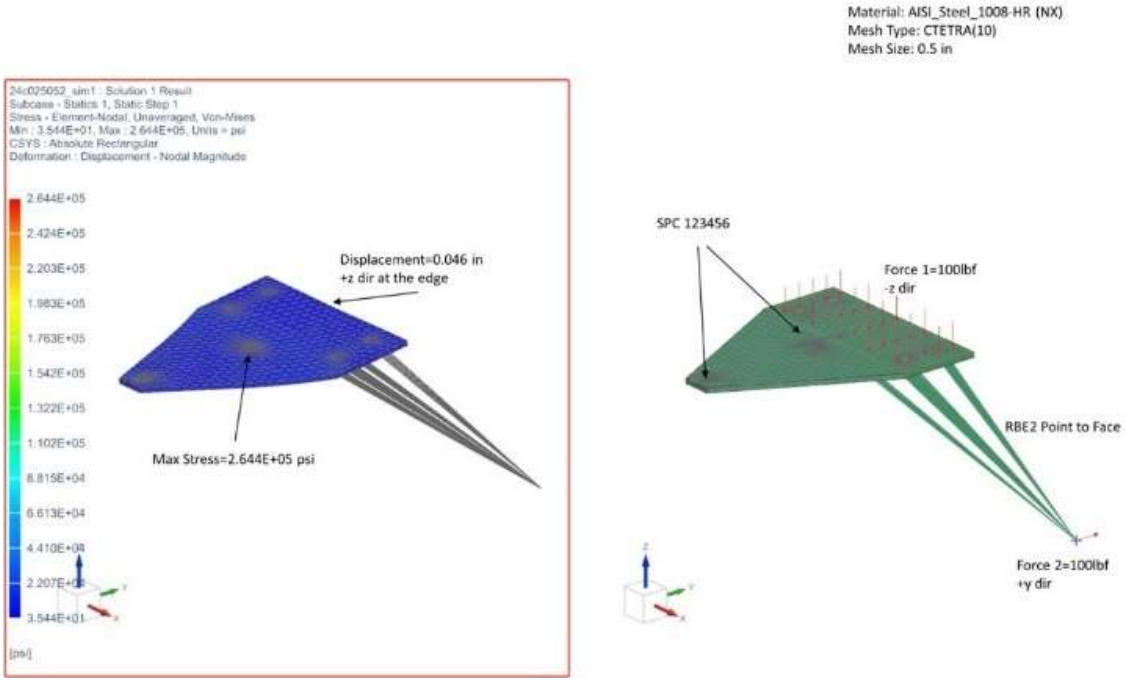

Fig. 1: FEA of loads on test plate, T-Bone Extension.

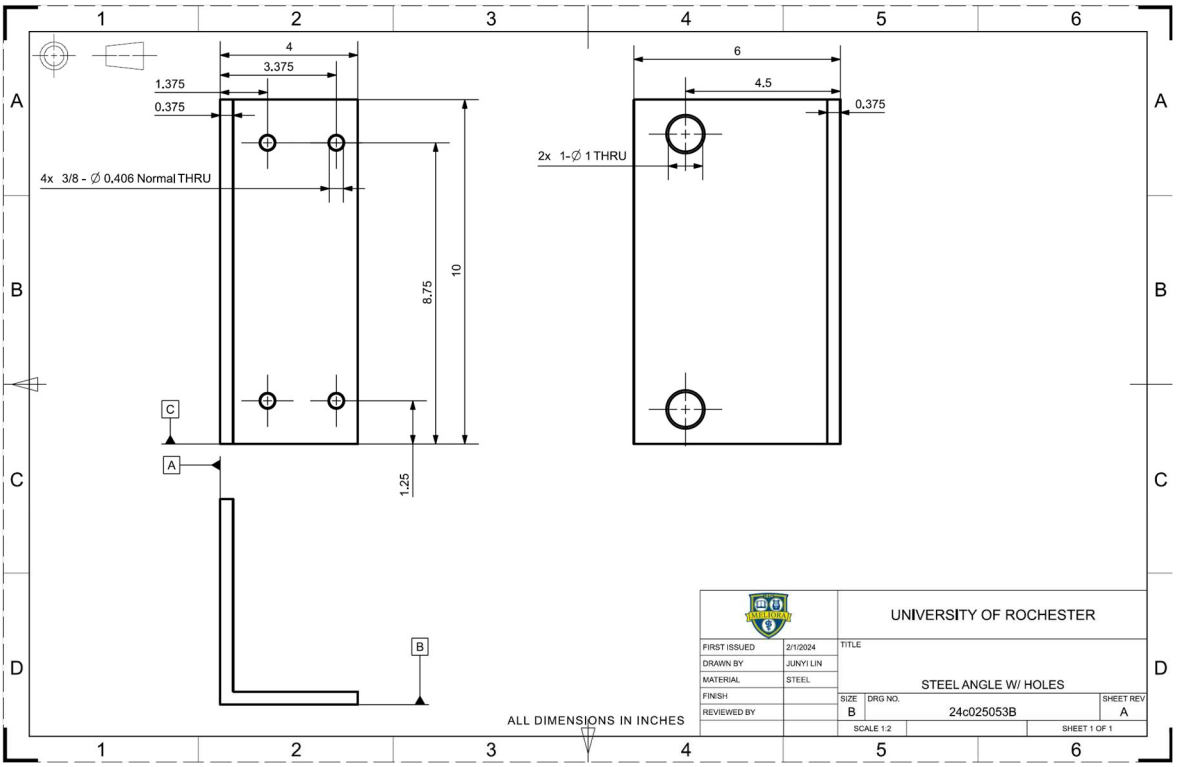

Fig. 2: Engineering drawing of testing rig, steel angle with holes.

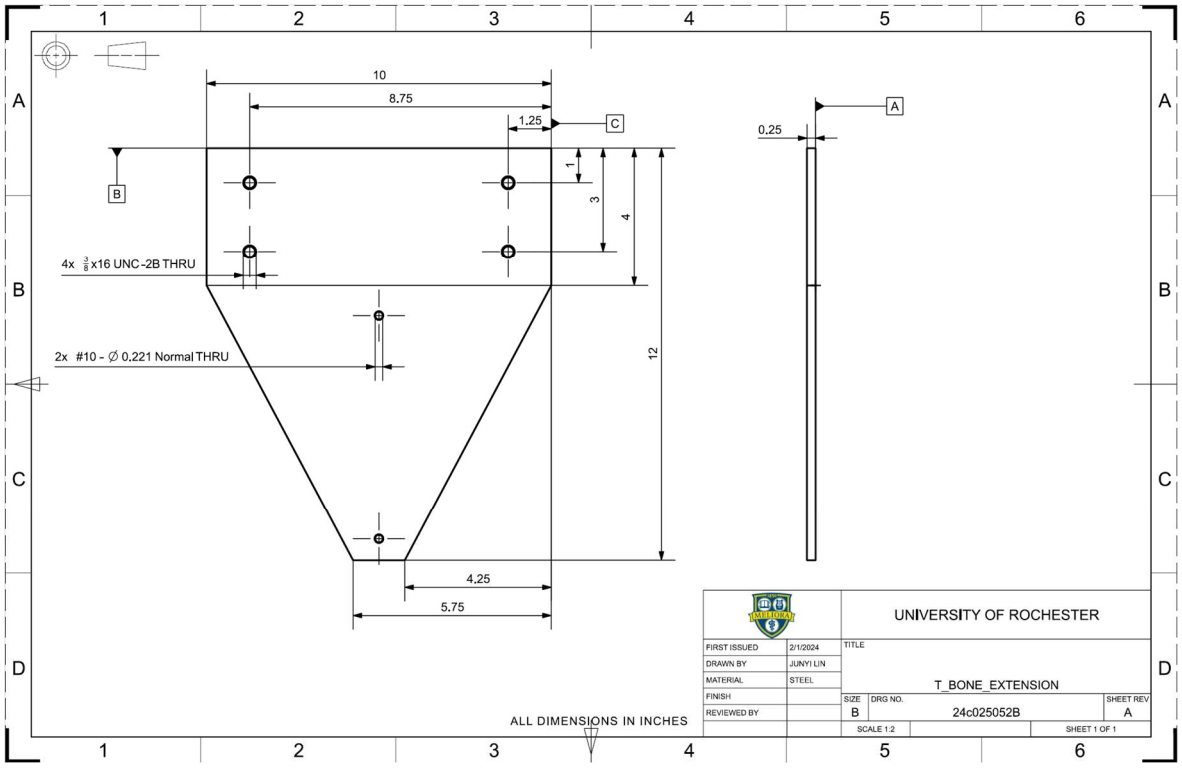

Fig. 3: Engineering drawing of testing rig, T-Bone extension.

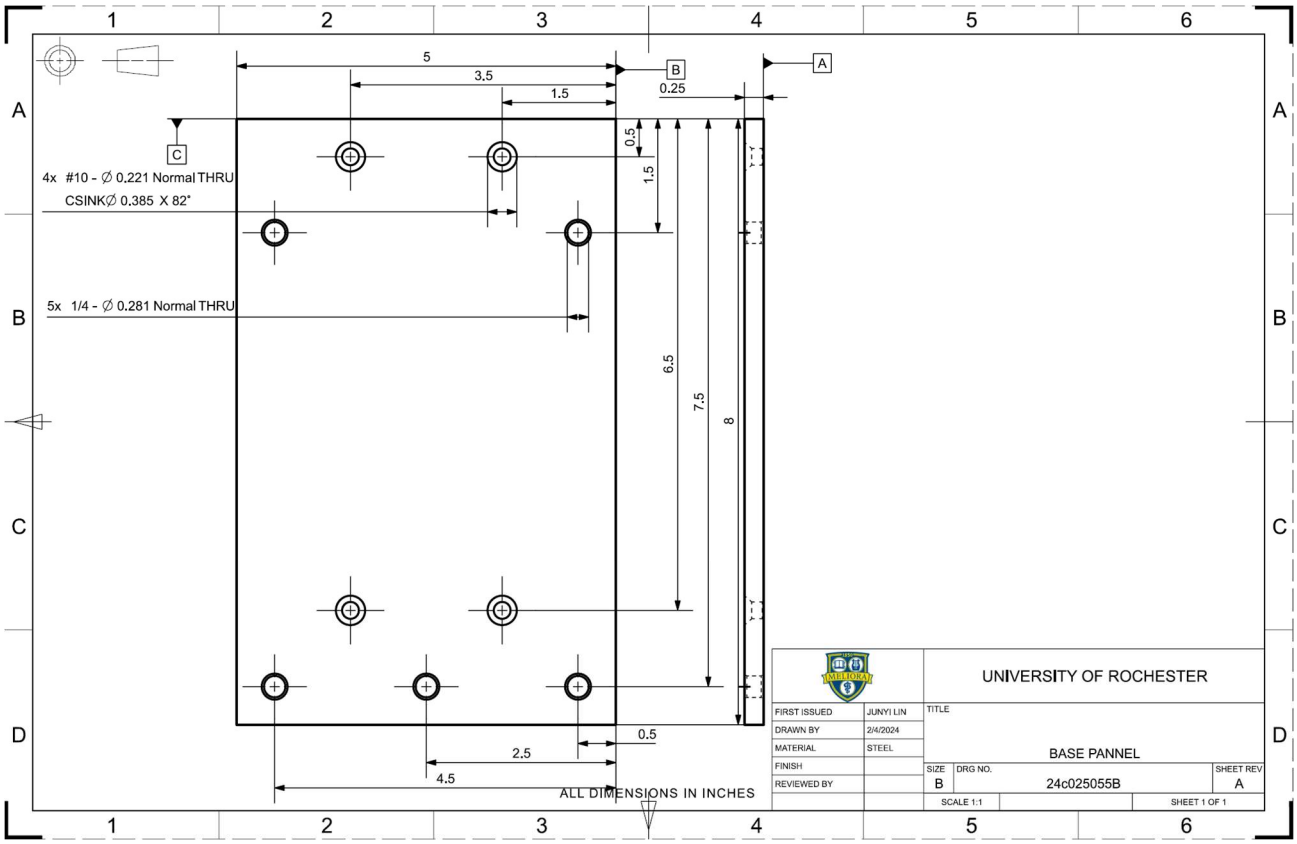

Fig. 4: Engineering drawing of testing rig, base panel.

Fig. 5: The motor mount and uniaxial slider in the testing rig.


Fig. 6: The assembled testing rig setup.

Fig. 7: The battery configuration used to power the motor.


Fig. 8: Testing on site.

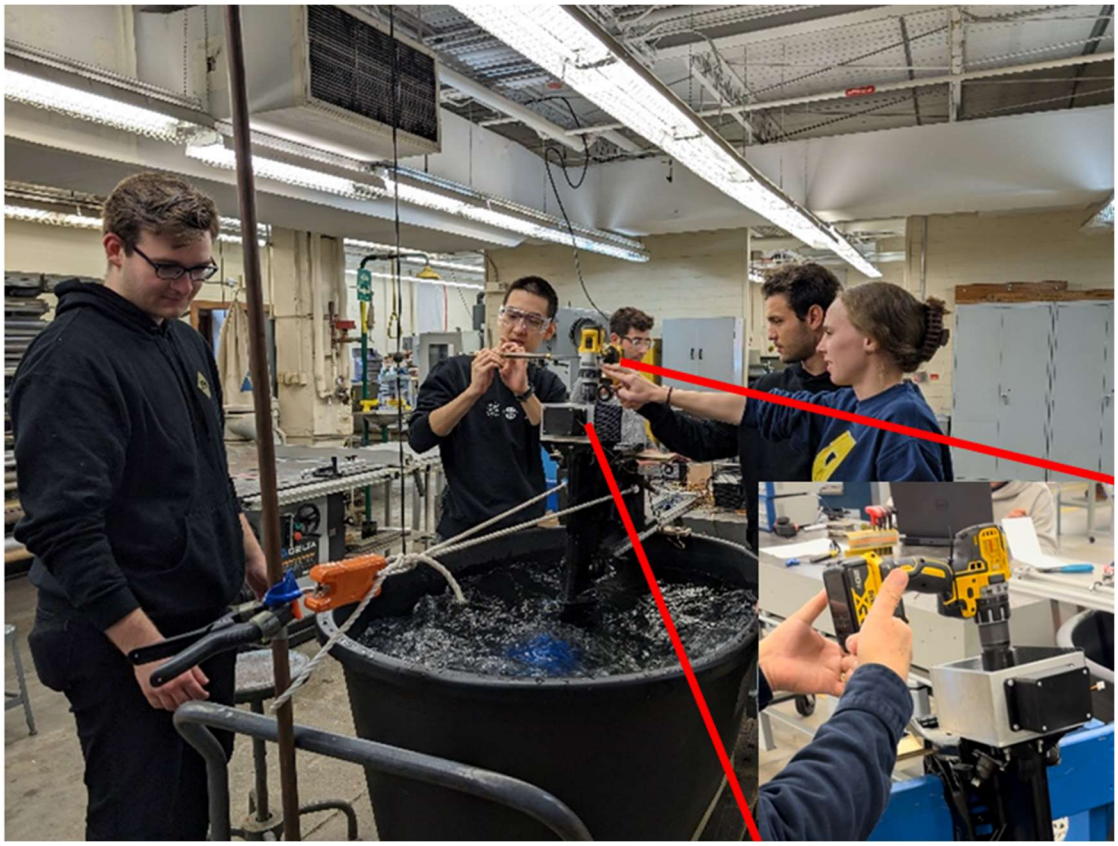

Fig. 9: Torque Testing.

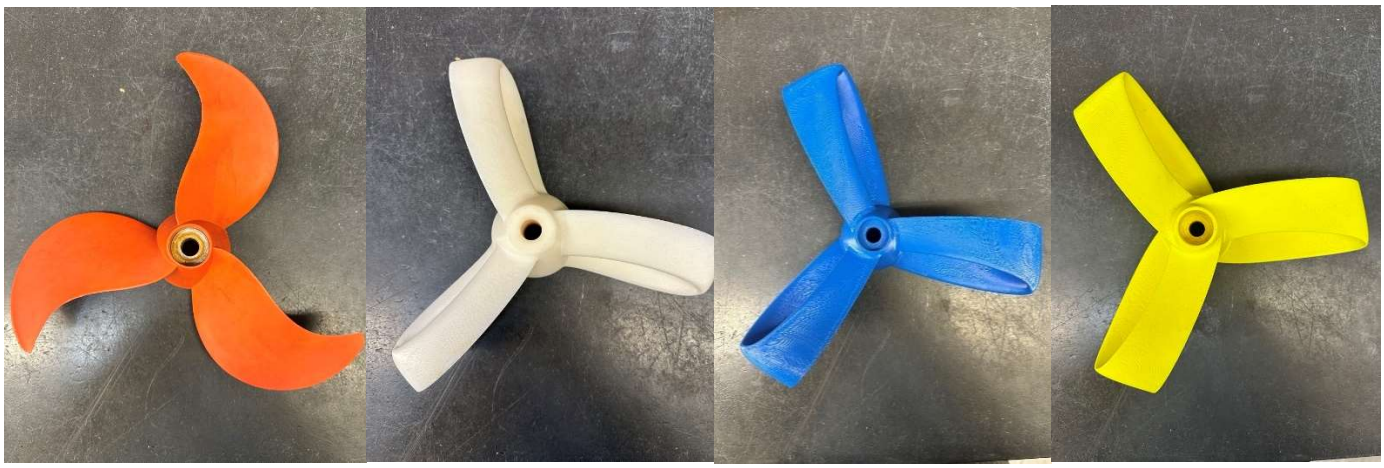

Fig. 10a: (Left) Solar Splash Propeller.
Fig. 10b (Left-Middle) Baseline Propeller.
Fig. 10c (Right-Middle) Local Maximum Propeller.
Fig. 10d (Right) Toroidal Propeller (Final Design).

APPENDIX C-PLOTS FOR TESTING

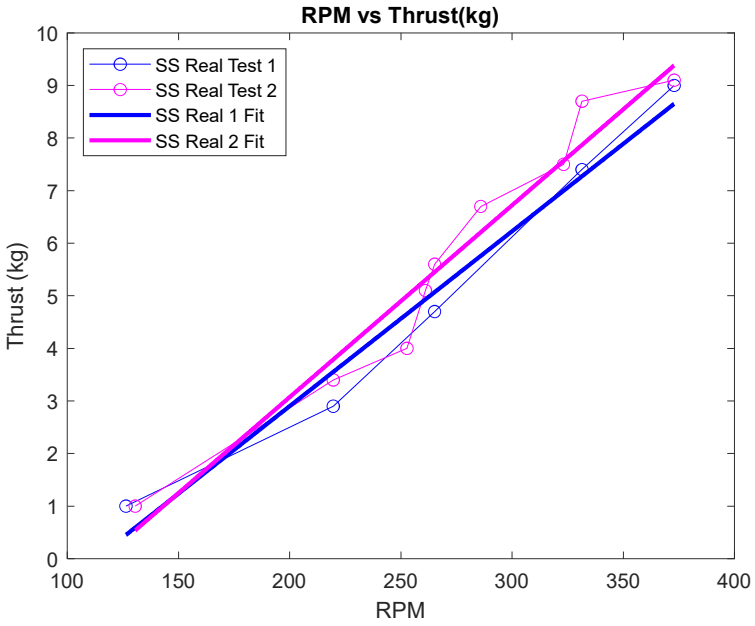

Fig. 11: RPM vs Thrust results for two different testing sessions on the Solar Splash propeller.

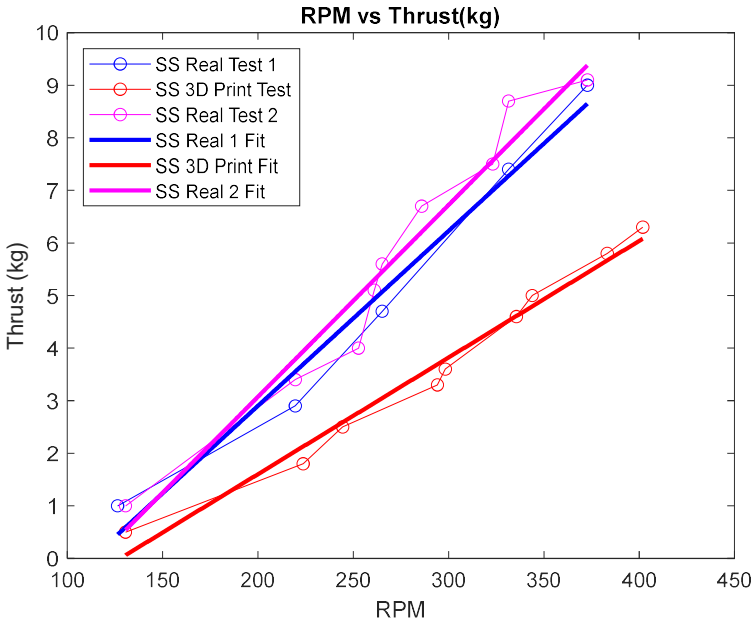

Fig. 12: Compare SS 3D printed to SS actual testing.

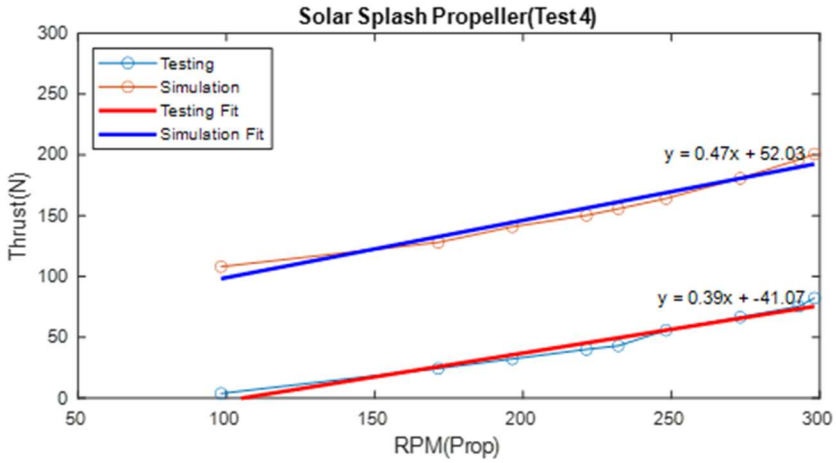

Fig. 13: Plot to compare trends in Solar Splash Simulation and Solar Splash testing data.

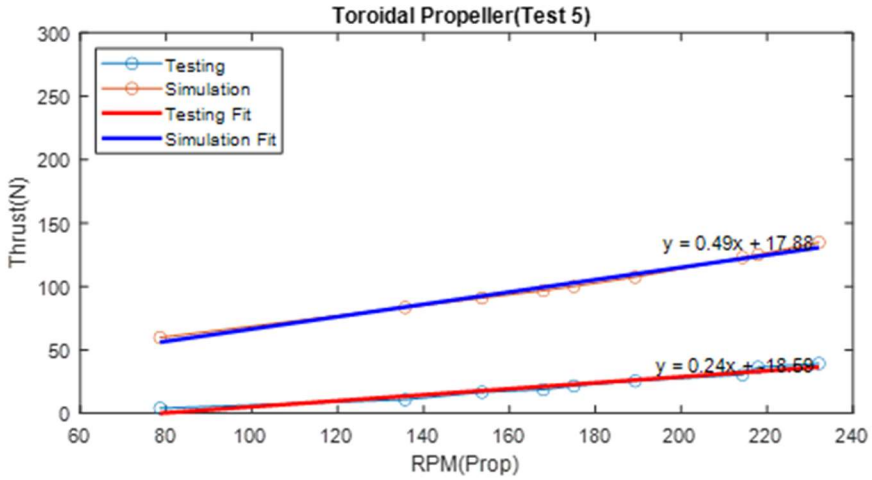

Fig. 14: Plot to compare trends in Toroidal simulation and Toroidal testing data.

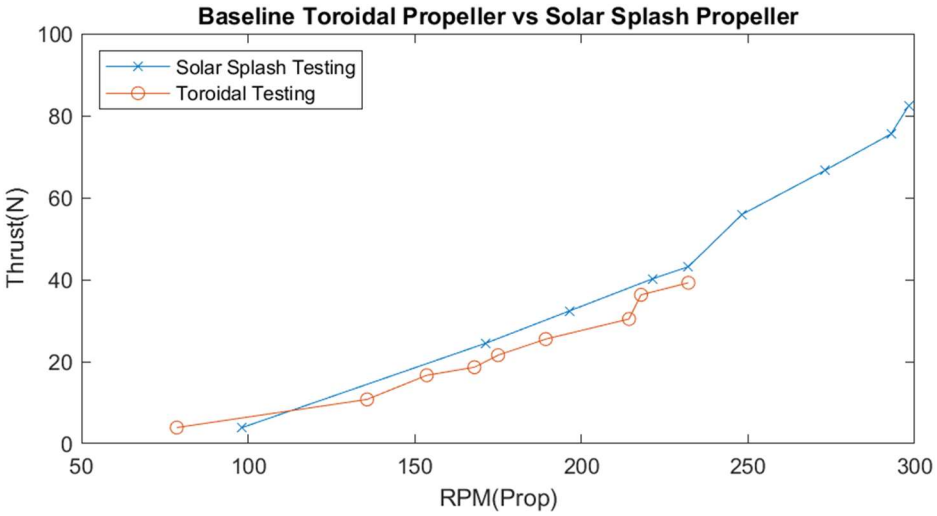

Fig. 15: Thrust vs. RPM plot for testing Solar Splash propeller and Baseline Toroidal propeller.

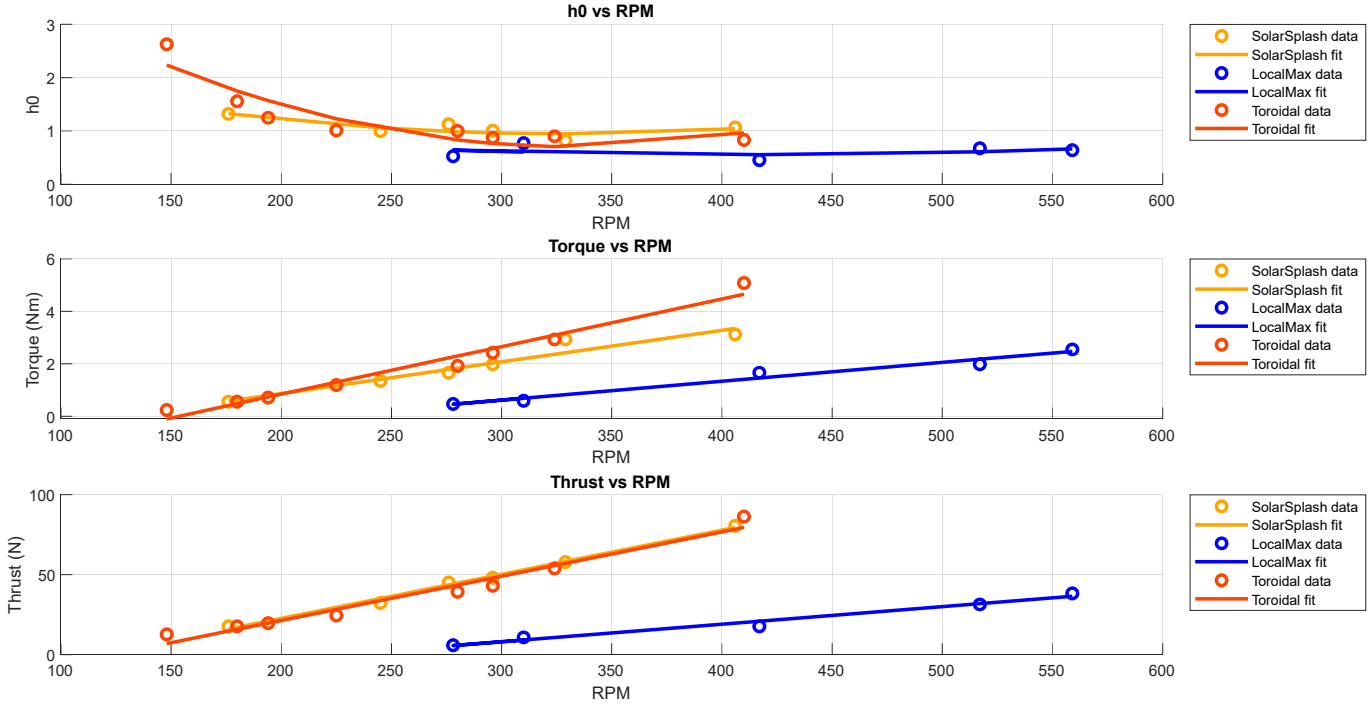

Fig. 16: Plots comparing Solar Splash propeller to Local Max Toroidal and Final Toroidal propellers in Testing.

TABLE 8
SOLAR SPLASH PROPELLER AMP DATA

ERPM	RPM (from ERPM)	% Difference	RPM (Prop)	Thrust (kg)	Thrust + Slack (N)	AMP
1550	128.4	2.78	132	0	3.92	5
2150	178.1	3.85	185	1.2	15.70	7.5
2550	211.3	4.12	220	2	23.54	10
3000	248.6	3.39	257	3	33.35	12.5
3300	273.4	4.96	287	4.2	45.13	15
3600	298.3	6.27	317	4.9	51.99	17.5
3900	323.1	5.22	340	6.2	64.75	20
4300	356.3	6.09	378	7.2	74.56	22.5

TABLE 9
TOROIDAL PROPELLER AMP DATA

ERPM	RPM (from ERPM)	%Difference	RPM (Prop)	Thrust (kg)	Thrust + Slack (N)	AMP
1225	101.5	4.43	106	0	1.96	5
1800	149.1	0.57	150	0	1.96	7.5
2300	190.6	3.37	197	1	11.77	10
2800	232.0	4.74	243	1.8	19.62	12.5
3000	248.6	5.00	261	2.5	26.49	15
3400	281.7	3.65	292	3.1	32.37	17.5
3600	298.3	3.93	310	3.6	37.28	20
3900	323.1	6.15	343	4.7	48.07	22.5

TABLE 10
SOLAR SPLASH PROPELLER TORQUE DATA

RPM (Prop)	Thrust w/ Slack (N)	Digital Scale (N)	Motor Torque (Nm)	Prop Torque (Nm)	Kt (Thrust Coe.)	Kq (Prop Torque Coe)	h0 (Open Water Efficiency)
176	17.66	1.95	0.321	0.55	0.447	0.054	1.321
245	32.37	4.73	0.781	1.35	0.423	0.067	0.997
276	45.13	5.84	0.964	1.66	0.464	0.066	1.125
296	48.07	6.95	1.148	1.98	0.430	0.068	1.007
329	57.88	10.29	1.699	2.93	0.419	0.081	0.819
406	80.44	10.96	1.809	3.12	0.383	0.057	1.069

TABLE 11
TOROIDAL PROPELLER TORQUE DATA

RPM (Prop)	Thrust w/ Slack (N)	Digital Scale (N)	Motor Torque (Nm)	Prop Torque (Nm)	Kt (Thrust Coe.)	Kq (Prop Torque Coe)	h0 (Open Water Efficiency)
148	12.75	0.83	0.138	0.24	0.235	0.014	2.627
180	17.66	1.95	0.321	0.55	0.220	0.022	1.559
194	19.62	2.50	0.413	0.71	0.285	0.036	1.249
225	24.53	4.17	0.689	1.19	0.196	0.031	1.010
280	39.24	6.73	1.111	1.92	0.202	0.032	1.002
296	43.16	8.51	1.405	2.42	0.199	0.036	0.872
324	53.96	10.29	1.699	2.93	0.207	0.037	0.901
410	86.33	17.85	2.948	5.08	0.207	0.040	0.831

TABLE 12
LOCAL MAXIMUM PROPELLER TORQUE DATA

RPM (Prop)	**Thrust w/ Slack (N)**	**Digital Scale (N)**	**Motor Torque (Nm)**	**Prop Torque (Nm)**	**Kt (Thrust Coe.)**	**Kq (Prop Torque Coe)**	**h0 (Open Water Efficiency)**
310	10.79	2.09	0.344	0.59	0.079	0.016	0.774
278	5.89	1.67	0.275	0.47	0.054	0.016	0.528
417	17.66	5.84	0.964	1.66	0.072	0.025	0.452
517	31.39	6.95	1.148	1.98	0.083	0.019	0.675
559	38.26	8.96	1.479	2.55	0.086	0.021	0.639

APPENDIX D-SIMULATION FIGURES

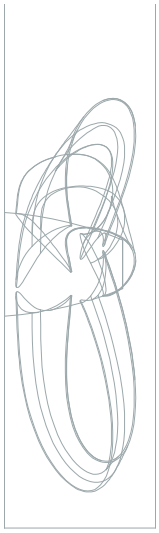

Fig. 17: Static wireframe view of rotating region geometry in NX

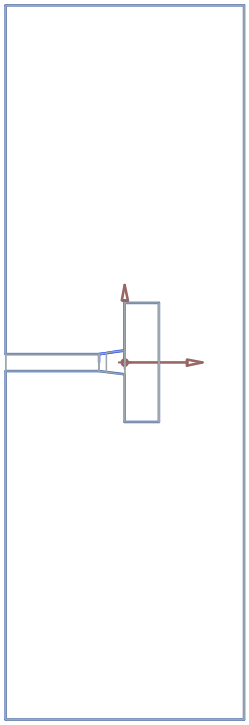

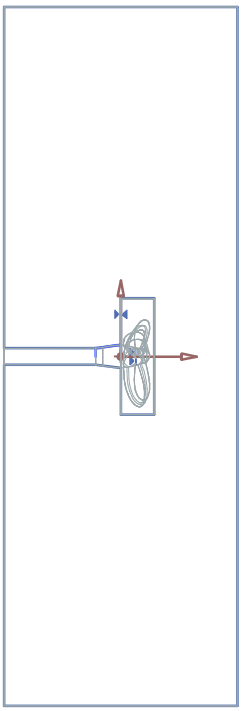

Fig. 18a (Left): Static wireframe view of static region geometry in NX
Fig. 18b (Right): Static wireframe view of assembly geometry in NX

APPENDIX E-OPTIMIZATION PLOTS

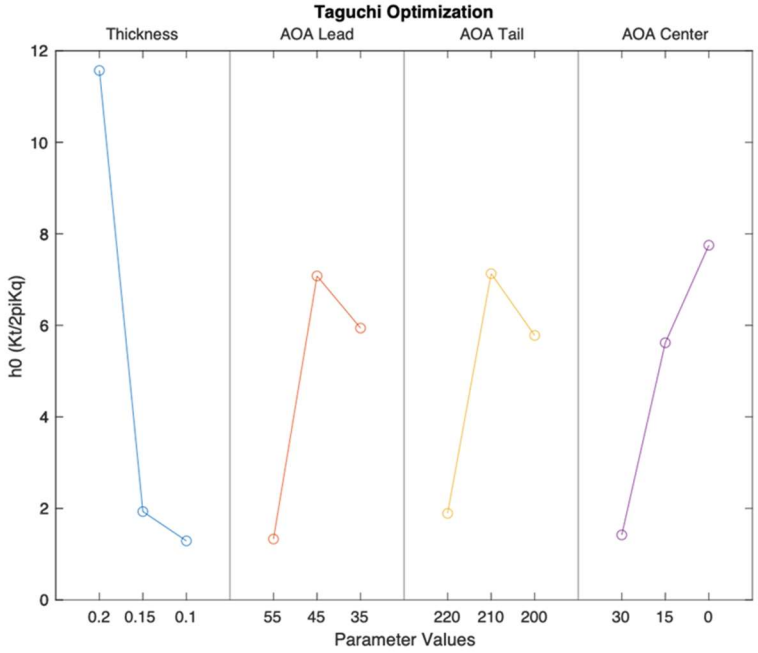

Fig. 19: Round one results of Taguchi Method optimization examining four parameters at three levels.

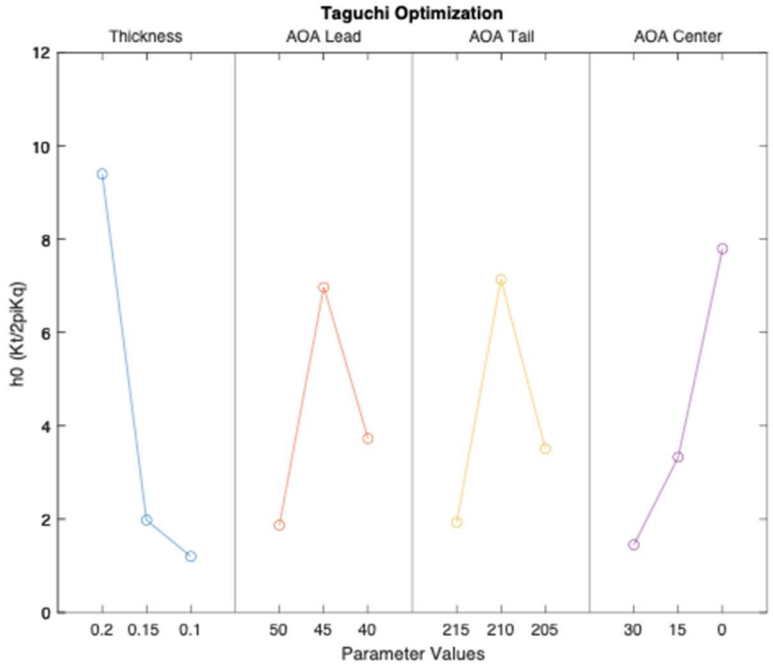

Fig. 20: Round two results of Taguchi Method optimization examining the same four parameters using narrowed range of values for AOA Lead and AOA Tail to investigate regions between data points.

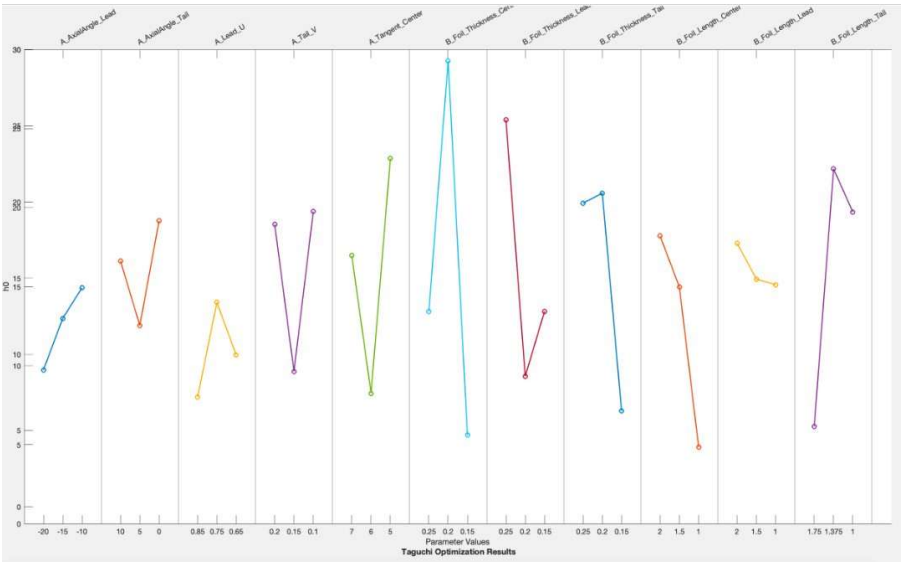

Fig. 21: Round two results of Taguchi Method optimization examining eleven parameters at three levels.

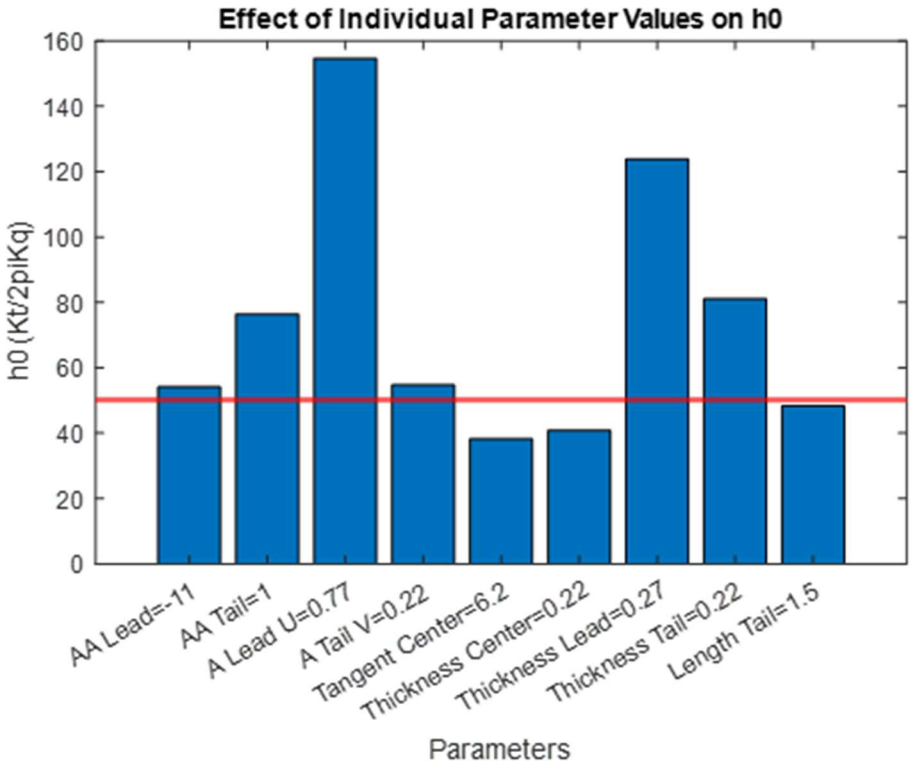

Fig. 22: Exploring the robustness of the local maximum.

APPENDIX F-NX MODEL

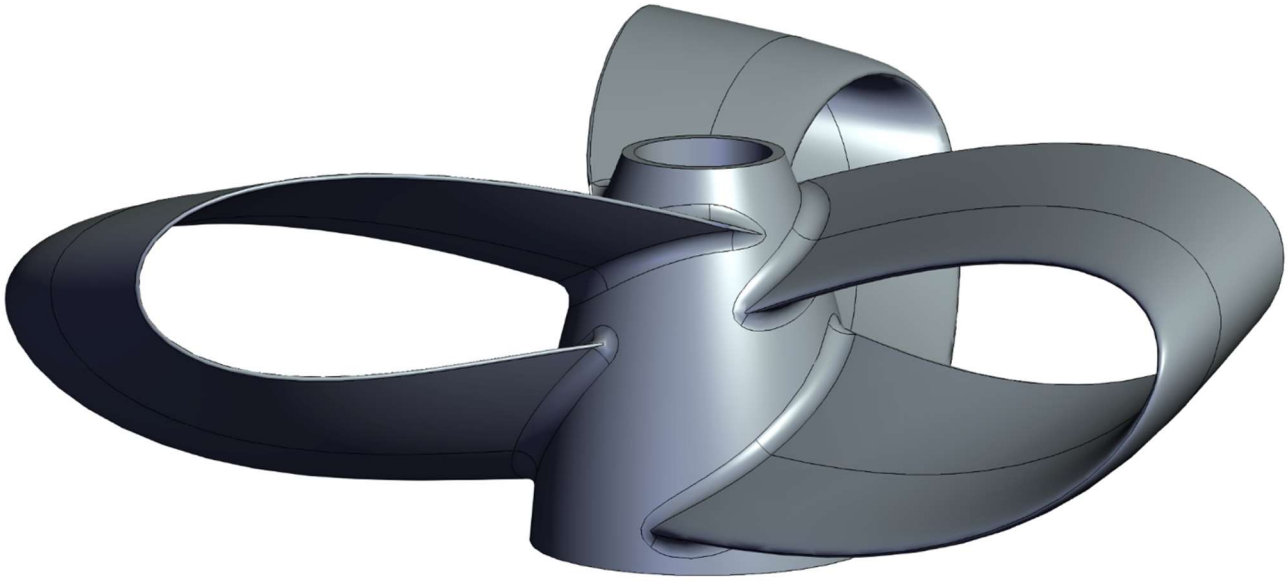

Fig. 23: Final toroidal propeller model.

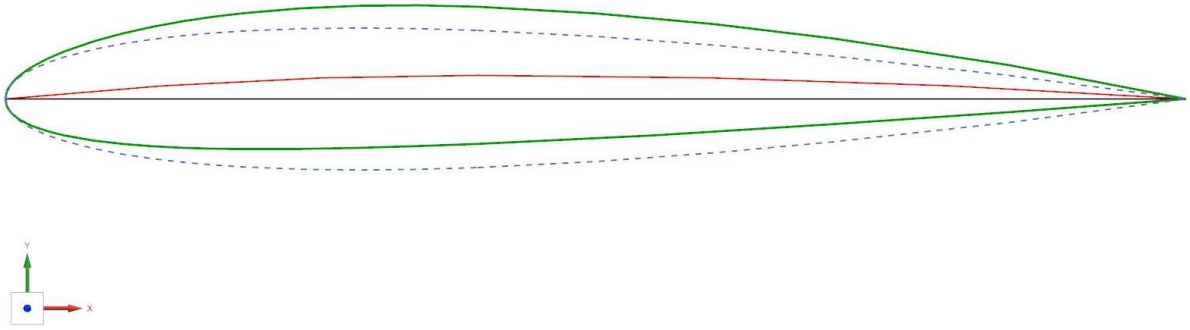

Fig. 24: NACA 2412 airfoil example with reference lines (Green: NACA 2412 Airfoil, Red: Camber Line, Dotted: NACA 0012 Airfoil)

APPENDIX G-THEORY OF OPERATION

INSTALLATION

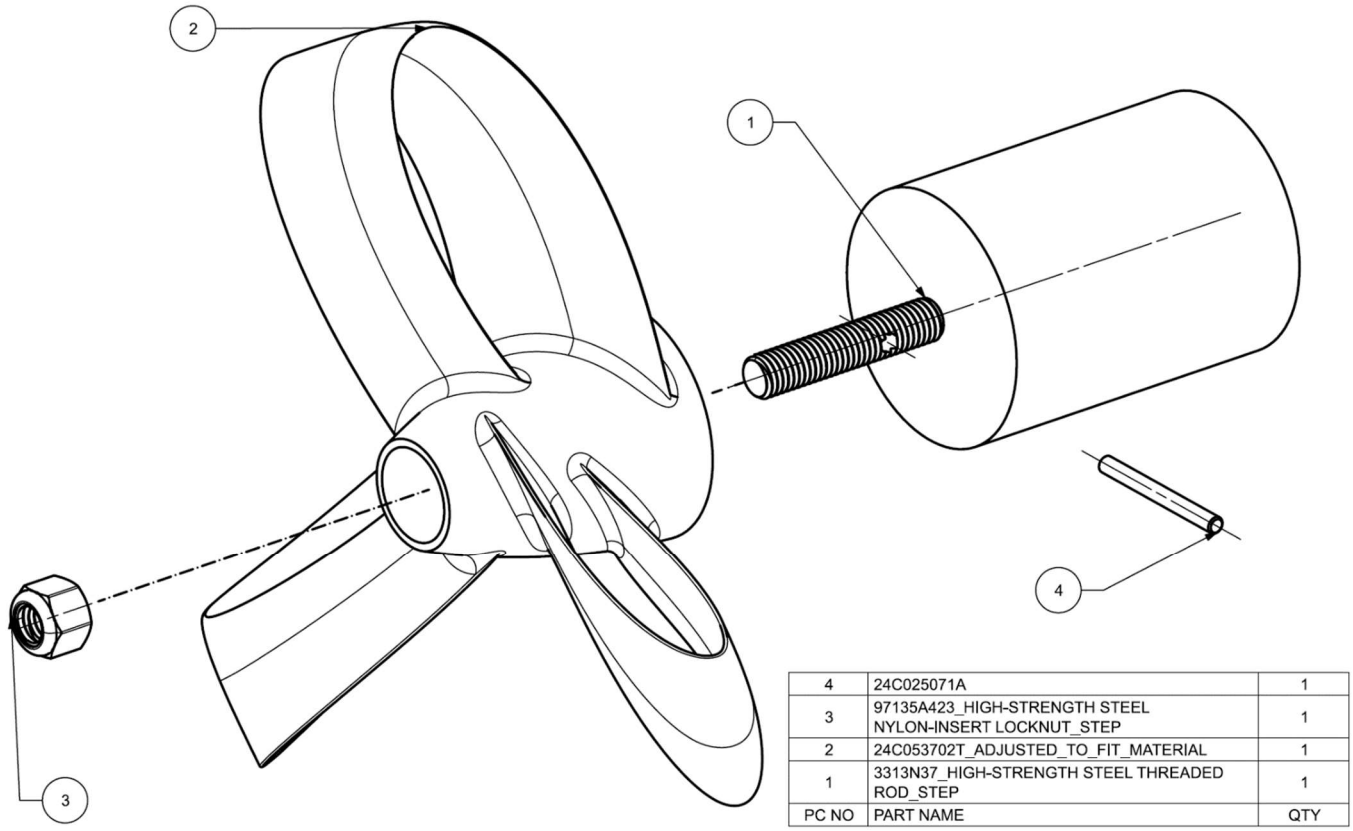

PC NO	PART NAME	QTY
4	24C025071A	1
3	97135A423_HIGH-STRENGTH STEEL NYLON-INSERT LOCKNUT_STEP	1
2	24C053702T_ADJUSTED_TO_FIT_MATERIAL	1
1	3313N37_HIGH-STRENGTH STEEL THREADED ROD_STEP	1

Fig. 25: Assembly of Propeller Mount

The installation of the toroidal propeller system is delineated in Fig. 25, showcasing an exploded view of the propeller assembly. This assembly is composed of four main components:

1. High-Strength Steel Threaded Rod (Part No. 3313N37): Serves as the central axis and connects the propeller to the drive shaft.
2. Toroidal Propeller (Adjusted to Fit Material, Part No. 24C053702T): The primary thrust-generating component, featuring a ring-shaped blade design for enhanced efficiency.
3. Nylon-Insert Locknut (Part No. 971354A23): Ensures the propeller remains securely fastened to the threaded rod, preventing loosening due to vibrations or rotational forces.
4. Shearing Pin (Part No. 24C025071A): A safety device designed to shear in the event of propeller overload or entanglement, protecting the drive system from damage.

The installation process involves attaching the threaded rod to the propulsion shaft, followed by sliding the toroidal propeller onto the rod, and securing the assembly with the nylon-insert locknut. The shearing pin is inserted as a final step to complete the assembly, providing a critical safety measure. This configuration is critical for achieving the intended operational performance, safety, and reliability of the toroidal propeller system.

When installing the toroidal propeller system, particular attention must be paid to the torque specifications for securing the nylon-insert locknut onto the 1/2-13 threaded rod. The 1/2-13 designation refers to a 1/2-inch diameter rod with 13 threads per inch, which is a standard size in fastening applications. Proper torque application ensures a secure fit that resists loosening from vibrations while avoiding excessive force that could strip the threads or damage the components. As recommended by the manufacturer [7], the torque applied to the nylon-insert locknut should be 41-61 ft-lb.

SAFETY PROTOCOLS

Ensuring the safety of all personnel and equipment involved in the operation and testing of the toroidal propeller is paramount. This protocols outline the comprehensive rues designed to mitigate risks and ensure a secure working environment. Our safety procedures align with the University of Rochester's standards and the mechanical engineering department's guidelines. By adhering to these protocols, we maintain not only compliance with institutional regulations but also a commitment to the wellbeing of the testing team and the integrity of our research.

- PPE – Safety Glasses
- Ensure the system is not energized.
- Check the area for overspray.
- Make sure the table wheels are locked.
- Make sure the propeller is properly attached.
- Make sure power supply, wires, and energized equipment are secure.
- Make sure the motor is properly attached.
- Make certain steering in locked.
- Adjust motor height and alignment, as necessary.
- Check electrical connections.
- Make certain force-measuring device is properly set up.
- Set rpm to zero.
- Power on and bring up speed.
- Take measurements.
- Slow down.
- Disconnect power.
- Check area for spillage.

APPENDIX H-PRESSURE FEA ANALYSIS

Fig. 26: Relative total pressure plot for the final toroidal model running at 5.5 rev/s (300RPM).

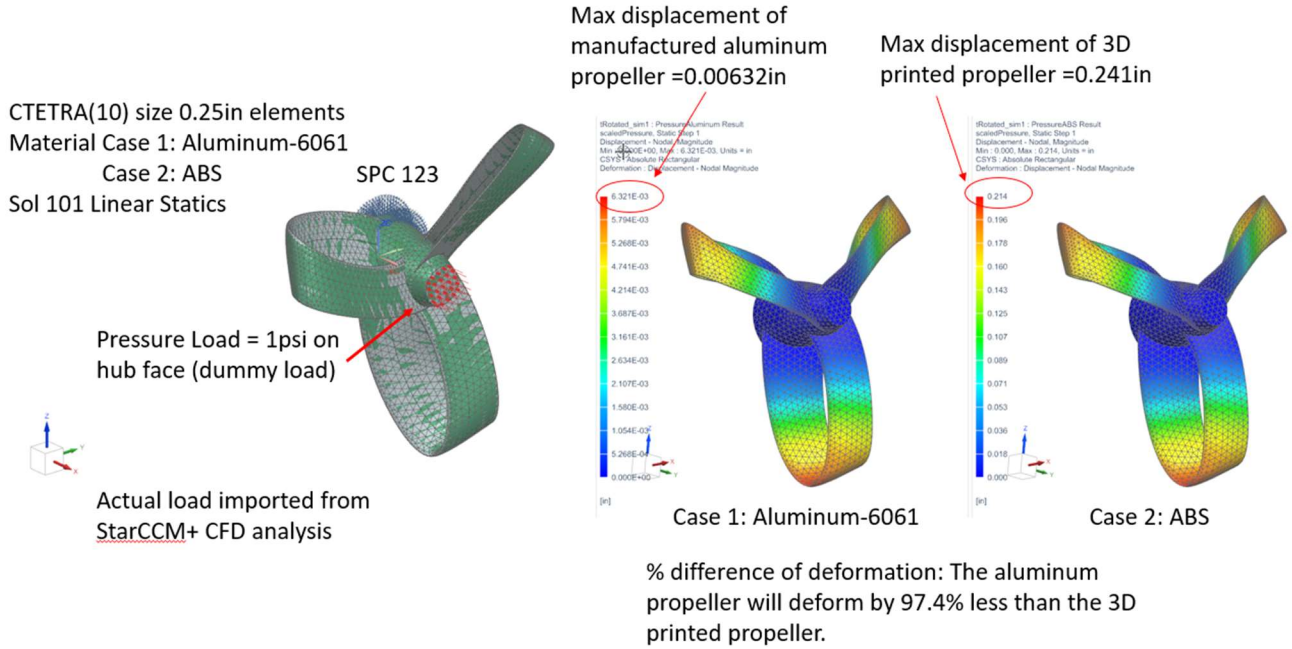

Fig. 27: One pager of Pressure FEA mapped from StarCCM+.

Explanation of Results:

The relative total pressure plot was outputted from a StarCCM+ simulation of the final toroidal propeller running at 300RPM. A mesh of the NX model was exported as a Nastran file and imported into StarCCM+. The pressure data from StarCCM+ was interpolated onto the NX mesh. A data file containing the pressure loads across the nodes and elements of the mesh was then exported. In NX, a dummy load of 1psi and the above constraints were added. In the Nastran solution file, the load case was replaced with the linked pressure load data file. Two solutions were created with the same boundary conditions and loads and the two material cases above. The aluminum 6061 manufactured case deforms 97% less than the ABS 3D printed case, indicating the propeller will perform better as aluminum 6061.

APPENDIX I-WORK BREAKDOWN STRUCTURE & CRITICAL PATH MANAGEMENT

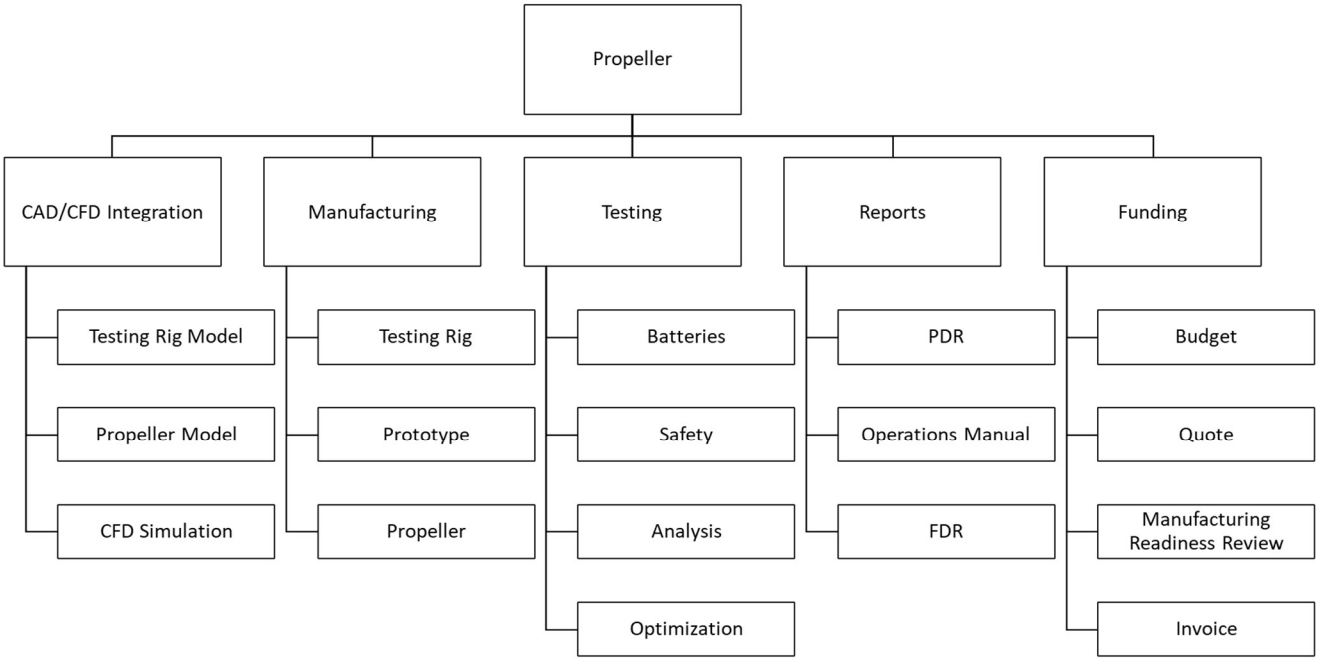

Fig. 28: WBS Chart with Major Deliverable Components

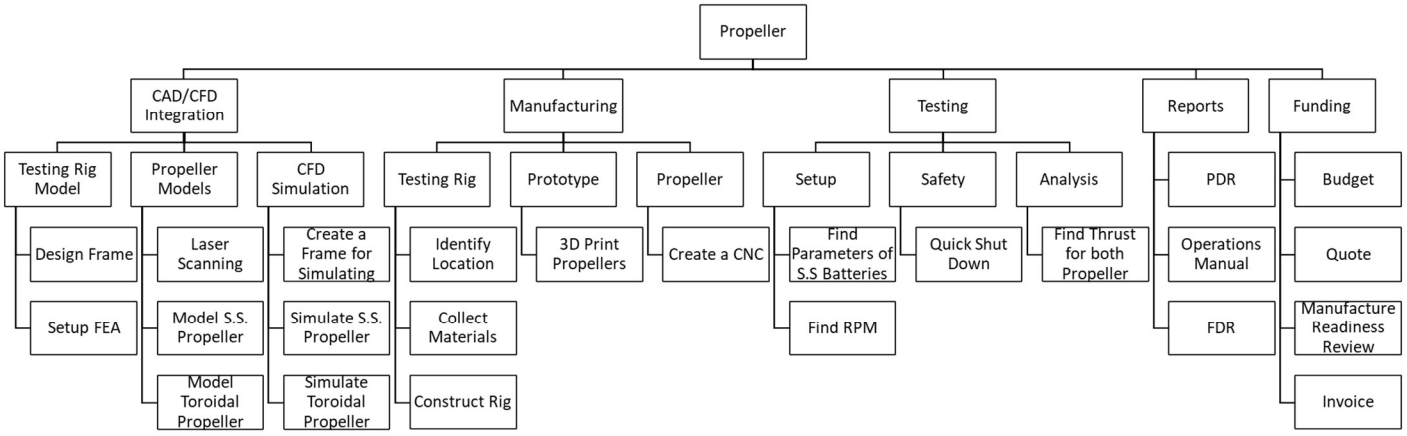

Fig. 29: WBS Chart with Activities for Deliverables

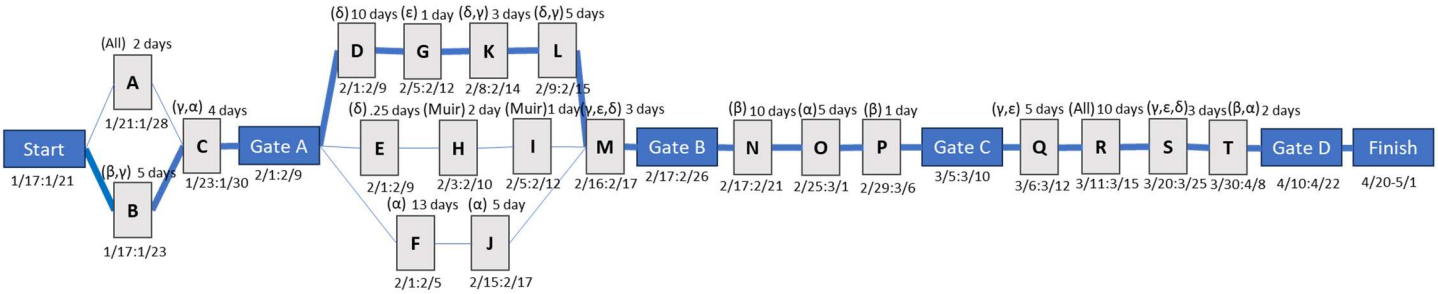

Fig. 30: CPM Chart for the project.

TABLE 13
CORRESPONDING TASK FOR CPM

Activities	**Duration (Days)**	**Cost ($)**	**Slack Time (Days)**
A. Meet with S.S. to discuss Parameters and their Requirements/Specifications	2	2000	3
B. Propeller Patent Search/Toroidal Propeller Design Research	5	5000	0
C. Assemble Requirements/Specifications	4	4000	0
D. Model Frame for Testing Rig	10	10000	0
E. Laser Scan S.S. original propeller model	.25	250	16
F. Create a CFD Simulation	13	13000	1
G. Setup FEA for Testing Rig	1	1000	0
H. Model S.S. original Propeller	2	2000	17.75
I. 3D Print S.S. original Propeller	1	1000	16.75
J. Simulate CFD for S.S. original Propeller	5	5000	6
K. Collect Materials and Parameters for Testing Rig (Voltage, Current, RPM)	3	3000	0
L. Fabricate Testing Rig (fabricate, program, power source)	5	5000	0
M. Test S.S original Design to determine Thrust and Efficiency	3	3000	0
N. Model Toroidal Propeller	10	10,000	0
O. Simulate CFD for Toroidal Propeller	5	5000	0
P. 3D Print scaled Toroidal Propeller (Frankenstein)	1	1000	0
Q. Write G-code	5	5000	0
R. Manufacture Toroidal Propeller in CNC Machine	10	10000	0
S. Test Toroidal Propeller to determine Thrust and Efficiency	3	3000	0
T. Write an Operations Manual for Toroidal Propeller	2	2000	0
	Total:	$90,250	
Resources			
Alpha (α) - Claire			
Beta (β) - Henry			
Gamma (γ) - Jacob			
Delta (δ) - Junyi			
Epsilon (ε) - Santino			